Counter-rotating eddy pair in the Luzon Strait

Sun Ruili[1,2*], Li Peiliang[1,3], GuYanzhen[3], Zhai Fangguo[4], Yan Yunwei[2], Li Bo[5]

[1]Hainan Institute of Zhejiang University, Sanya, Hainan, China

[2]State Key Laboratory of Satellite Ocean Environment Dynamics, Second Institute of Oceanography, Ministry of Natural Resources, Hangzhou, China

[3]Ocean college, Zhejiang University, Zhoushan, China

[4]College of Oceanic and Atmospheric Sciences, Ocean University of China, Qingdao, China

[5]State Key Laboratory of Tropical Oceanography, South China Sea Institute of Oceanology, Chinese Academy of Sciences, Guangzhou, China

Corresponding author：Sun Ruili, sunruili2007@126.com

Abstract:

Based on satellite remote ~~-~~sensing observation data and Hybrid Coordinate Ocean Model (HYCOM) ~~reanalysis~~re-analysis data, we studied the counter-rotating eddy pair in the Luzon Strait (LS). Statistical analysis ~~revealed~~reveals that when an ~~anticyclonic~~anti-cyclonic mesoscale eddy (AE) (cyclonic mesoscale eddy ~~(~~[CE~~)~~]) in the Northwest Pacific (NWP) gradually ~~approached~~approaches the east side of the LS, a CE (an AE) gradually ~~formed~~forms on the west side of the LS, and it ~~was~~is defined as the AE (CE) mode of the counter-rotating eddy pair in the LS. The counter-rotating eddy pair ~~exhibited~~exhibits obvious seasonal variation: the AE mode mainly ~~occurred~~occurs in the summer half of the year, while the CE mode mainly ~~occurred~~occurs in the winter half of the year. The mean durations of the AE ~~mode~~ and CE ~~mode were~~modes are both ~~about~~approximately 70 ~~days~~d. Based on ~~energy analysis and the~~ vorticity budget equation and

Style Definition: 未处理的提及1
Style Definition: Unresolved Mention1
Formatted: Highlight
Formatted: Highlight
Formatted: Highlight
Formatted: Highlight
Formatted: Highlight

energy analysis, the dynamic mechanism of ~~the~~ counter-rotating eddy ~~-~~ pair occurrence ~~was~~is determined to be as follows: the AE (CE) on the east side of the LS causes a positive (negative) vorticity anomaly through horizontal velocity shear on the west side of the LS, and the positive (negative) vorticity anomaly is transported westward by the zonal advection of the vorticity, finally leading to the formation of the CE (AE) on the west side of the LS.~~–~~

Keywords: counter-rotating eddy pair; Luzon Strait; vorticity budget equation; barotropic instability~~;~~

1 Introduction

The Luzon Strait (LS), located between the island of Taiwan ~~Island~~ and ~~the~~ Luzon Island, is an important gap for ~~material~~particle and energy exchange between the South China Sea (SCS) and ~~the~~ Northwest Pacific (NWP). The topography around the LS is very complicated. The LS ~~comprises~~ is composed of three straits from north to south: ~~the~~ Bashi Strait, ~~the~~ Balintang Strait, and ~~the~~ Babuyan Strait. The Batanes Islands and Babuyan Islands are located in these ~~straights~~straits (Figure 1). ~~These~~This complex ~~topographic features can significantly affect the~~ topography leads to the generation and aggregation of a large number of mesoscale eddies, which then play an important role in the dynamic ocean process around the LS ~~and play an important role in the material and energy exchange between the SCS and the NWP (~~(Liu *et al*., 2012; Lu and Liu, 2013; Sun *et al*., 2016a)~~.~~; Sun *et al* ~~(2016a) pointed out that the Kuroshio bifurcates into west and east branches when it encounters the Batanes Islands in the LS. The bifurcation of the Kuroshio can significantly alter the transport of the Kuroshio's main axis, and therefore, it has a potential impact on the intrusion of the Kuroshio into the SCS. The bifurcation of the Kuroshio is also affected by mesoscale eddies (Sun et al~~., ~~2016a).~~ 2020).

Formatted: Highlight
Formatted: Highlight
Formatted: Highlight
Formatted: Highlight
Formatted: Font colour: Blue, Highlight
Formatted: Highlight
Formatted: Highlight
Formatted: Highlight
Formatted: Highlight
Formatted: Highlight
Formatted: Font: Italic, Highlight
Formatted: Highlight
Formatted: Highlight
Formatted: Font: Italic, Highlight
Formatted: Highlight
Formatted: Highlight

Mesoscale eddies widely exist in the vicinity of the LS, and many of them come from the NWP. These mesoscale eddies from the NWP can carry an enormous amount of kinetic energy and can alter the local circulation, including the Kuroshio. Some of them cross the LS into the SCS, thus contributing to the material and energy exchange between the SCS and the NWP. However, in addition to their method of entering the SCS, itinteraction is an important to determine if the mesoscale eddies from the NWP affect the material and energy exchange between the SCS and WNP in other ways? For example, mesoscale eddies from the NWP do not have to enter into the SCS, and they can affect the SCS circulation through eddy-eddy interactions.

Numerousfocus of previous studies have been conducted on the eddy-eddy interactionsmesoscale eddies in the vicinity of the LS. Jing and Li (2003) used satellite remote -sensing observation data to discover a cyclonic mesoscale cold eddy around the Lanyu Island to the northeast of the LS, and they speculated. They pointed out that the overshooting formation of the Lanyu cold eddy was the result of the joint action of the meandering Kuroshio when it leaves the SCS and the effects of the overshooting and conservation of the potential vorticity may be the formation mechanism of the Lanyu cold eddy. Using a neural network and satellite remote sensing observation data, Yin et al. Sun *et al*. (2014) statistically demonstrated that a CE (AE) from the NWP can decrease (increase) the velocity of the Kuroshio, thus causing the Kuroshio to intrude into the East China Sea (ECS) in a stronger (weaker) cyclonic manner. This showed that mesoscale eddies from the NWP can alter the ECS circulation without entering the ECS. Sun et al (2016b) believed that the formation of the Lanyu cold eddy was a process of eddies-eddies interaction. They used updated satellite remote sensing observation data and composition analysis to determinestudy the Lanyu cold-eddy phenomenon, and pointed out that the combined action of the Kuroshio loop (cyclonic circulation) and an AE from the NWP led to the formation of the Lanyu cold eddy ~~to the northeast of the LS. However, none of these studies determined the dynamic mechanism of eddy-eddy interactions.~~. Based on satellite observation data, *in situ* observation data and numerical modelling data, Zhang *et al.*, ~~(2007)~~(2017) studied mesoscale eddies-eddies interaction to the northwest of the LS. They analyzed the energy budget of the Kuroshio invading the SCS, and ~~they~~ determined that the northern branch of the ~~anticyclonic~~anti-cyclonic circulation caused by the Kuroshio loop ~~has~~had a large horizontal shear stress and thus ~~leads~~led to the formation of a CE southwest of ~~the~~ Taiwan Island through the barotropic instability~~, which proposed a dynamic mechanism for eddy-eddy interactions around the LS~~.

~~Although some research related to eddy-eddy interactions in the vicinity of the LS has been conducted, and it has been discovered that mesoscale eddies are widely distributed on the west and east sides of the LS (Figure 2), it is not clear whether the mesoscale eddies on the west and east sides of the LS can interact and exchange energy between the SCS and the NWP. In order to~~ Previous studies showed that mesoscale eddies-eddies interaction can cause particle and energy exchange and often occurs in the vicinity of the LS (Sun *et al.*, 2016b; Zhang *et al.*, 2017; Sun *et al.*, 2018). Since the LS is an important gap for particle and energy exchange between the SCS and NWP, a logical question is whether this phenomenon of mesoscale eddies-eddies interaction can occur on the east and west sides of the LS and whether it plays an important role in the particle and energy exchange between the SCS and NWP. To explore this issue, we ~~compared the~~compare sea~~-~~-surface height anomaly (SSHA) distributions in the SCS when a CE ~~occurred~~occurs and when an AE ~~occurred~~occurs on the east side of the LS (Figure ~~3~~2). The specific process ~~will be~~is described in detail in Section 3.1. Figure ~~3~~2 shows that when an AE (a CE) ~~occurred~~occurs on the east side of

Formatted: Highlight

Formatted: Font: Italic

Formatted: Highlight

Formatted: Font: Italic, Highlight

Formatted: Highlight

the LS, a CE (an AE) ~~formed~~forms on the west side of the LS, which was observed in the *in situ* observation data (Huang *et al.*, 2019). This is referred to in this article as the counter-rotating eddy-pair phenomenon~~ in this paper. This counter-rotating eddy pair process inevitably led to energy exchange between the SCS and the NWP. To the best of~~.

To our knowledge, ~~it is not only a new phenomenon proposed for~~ this is the first time~~, but it is also a new mechanism~~ a counter-rotating eddy-pair phenomenon in the LS has been proposed~~ for the first time, i.e., that~~, which creates a new form of particle and energy ~~is exchanged~~exchange between the SCS and the NWP. The present study will supplement and perfect the theory of particle and energy exchange between the SCS and NWP. We ~~analyzed~~give the statistical characteristics and dynamic mechanism of this phenomenon herein. The rest of this paper is organized as follows. Section 2 briefly introduces the data and methods~~.~~, Section 3 presents the research results~~.~~, and Section 4 ~~presents the~~provides a discussion and conclusion.

Formatted: Font: Italic
Formatted: Font: Italic
Formatted: Highlight
Formatted: Highlight
Formatted: Highlight
Formatted: Highlight
Formatted: Highlight
Formatted: Highlight
Formatted: Highlight

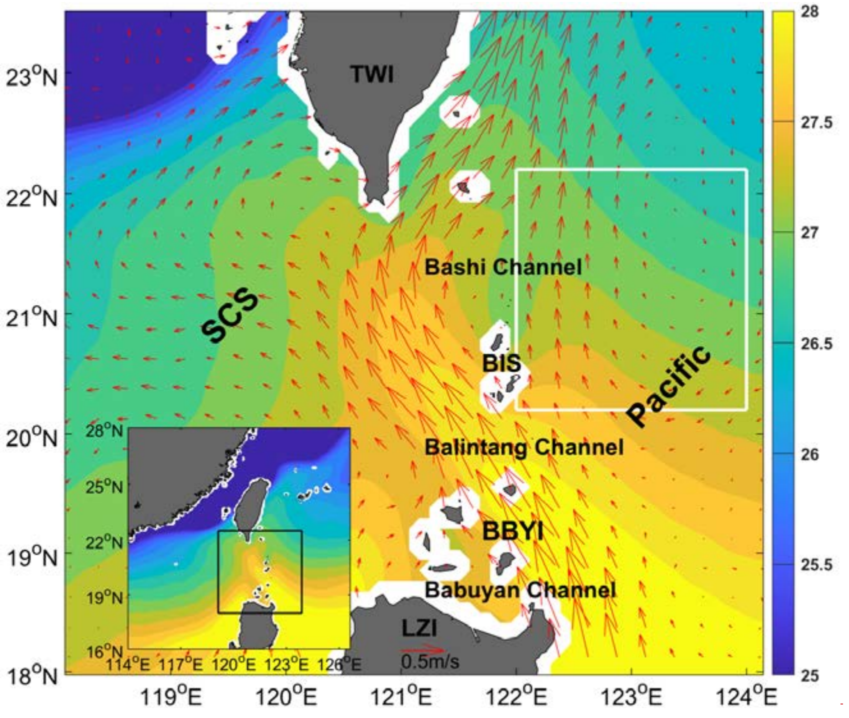
TWI
Bashi Channel
SCS
BIS
Pacific
Balintang Channel
BBYI
Babuyan Channel
LZI
0.5m/s
23°N
22°N
21°N
20°N
19°N
18°N
119°E
120°E
121°E
122°E
123°E
124°E
28
27.5
27
26.5
26
25.5
25
28°N
25°N
22°N
19°N
16°N
114°E
117°E
120°E
123°E
126°E

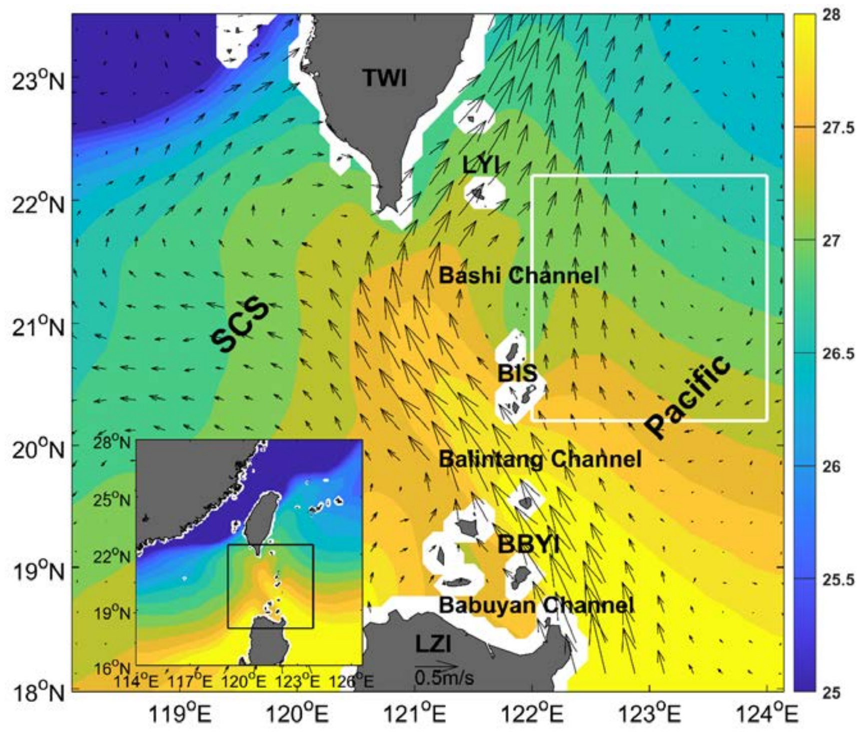

Figure 1. ~~Spatial~~Climate state of spatial distribution of ~~the~~ RSS SST (~~℃ ;~~°C; shading) and CMEMS geostrophic current (m/s; vectors), from 2003 to 2020. SCS~~:~~, South China Sea; BIS~~:~~, Batanes Islands; TWI~~:~~, Taiwan Island; LZI~~:~~, Luzon Island; BBYI~~:~~, Babuyan Islands~~. The white~~; LYI, Lanyu Island. White box borders 20.2~~-~~–22.2°N, 122~~-~~–124°E. ~~The extent~~Extent of the main map is shown as ~~a~~ black~~-~~bordered box in ~~the~~ inset.

Formatted: Highlight

Formatted: Highlight

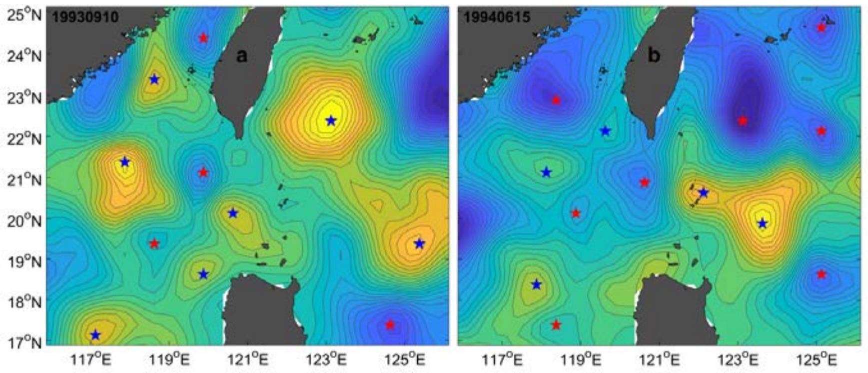

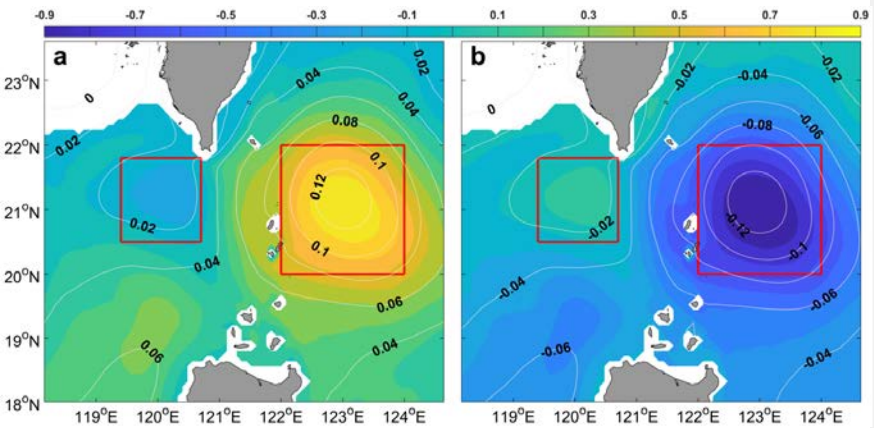

Figure 2. Spatial distribution of the CMEMS SSHA and locations of centers of the eddies on (a) September 10, 1993 and (b) June 15, 1994. The colors and contours represent the SSHA. The blue star and red star denote the locations of the AE and CE, respectively.

Formatted: Highlight

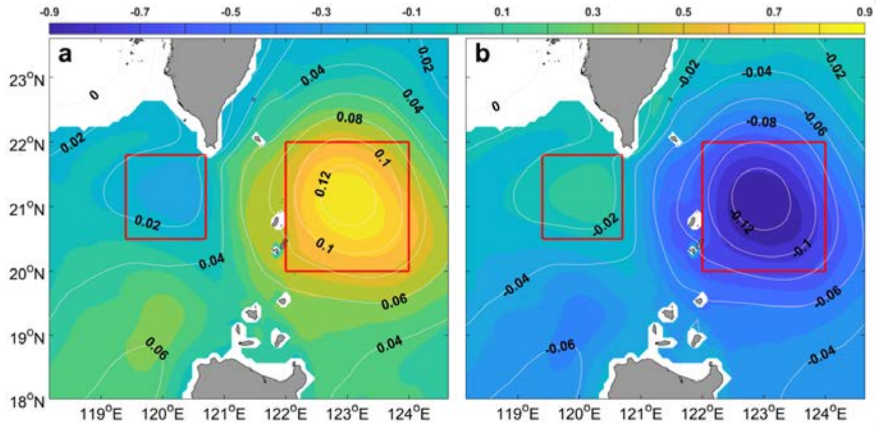

Figure 3. Spatial distribution of the counter-rotating eddy pair in the LS. (a) Spatial patternpatterns of the AE mode;(a) and CE (b) modes. Panel a (b) Spatial pattern of the CE mode. The contourscorresponds to average state when an AE (a CE) occurred in area marked by red box on east side of LS from 1993 to 2020. Contours represent SSHA (units of m). Colors represent the SSHA (unit: m). The colors represent the sea temperature anomaly (unit:℃units of °C) at a depth of 300 m. The intervalInterval of the SSHA is 0.03 m. The redRed boxes on the west side and east sidesides of the LS border mark 20.5–21.8°N, 119.4–120.7°E and 20–22°N, and 122–124°E, respectively. This figureFigure is similar to Figure 3 inof Sun *et al.* (2018), and is based on HYCOM data.

2 Data and methods

2.1 Data

Satellite remote-sensing SSHA, geostrophic current, and geostrophic current anomaly data arewere provided by the Copernicus Marine Environment Monitoring Service (CMEMS) (the download website: https://resources.marine.copernicus.Eu/?option=com_csw&view=details&product_id=

Formatted: Highlight

Formatted: Highlight

Formatted: Font: Italic

Formatted: Indent: First line: 0.74 cm

~~SEALEVEL_GLO_PHY_L4_REP_OBSERVATIONS_008_047).~~). The ~~data set is~~dataset was generated by the processing system including data from all altimeter missions: Sentinel-3A/B, Jason-3, HY-2A, Cryosat-2, OSTM/Jason-2, Jason-1, Topex/Poseidon, Envisat, GFO, and ERS-1/2. The ~~data set~~dataset provides ~~a~~ global coverage data from ~~1~~ January 1, 1993 to ~~present~~August 2, 2021, with a spatial resolution of 0.25°×0.25° and temporal sampling frequency of 1 ~~day~~d. It also provides one near-real-time component and one delayed-time component. The delayed-time component has been inter-calibrated and ~~provided~~provides a homogeneous and highly accurate, long time series of all altimeter data (Pujol and Francoise, 2019), and is chosen for use in this paper.

Model data are obtained from the Hybrid Coordinate Ocean Model (HYCOM) ~~organization provided the HYCOM reanalysis data (~~model output by the ~~download website: https://www.hycom.org/dataserver/gofs-3pt0/reanalysis).~~U.S. Naval Research Laboratory. The ~~data set~~dataset is based on ocean prediction system output, and the product with the longest time span from 2 October 1992 to 31 December 2012~~, is~~ was chosen ~~among~~from all HYCOM data-assimilation ~~product~~products provided by the HYCOM organization. The ~~data set~~dataset is based on ocean prediction system output with a spatial resolution of 0.08°×0.08° and 40 standard z-levels between 80.48°S and 80.48°N. It provides temperature, salinity, sea surface height, zonal flow, and meridional flow~~.~~ (Wallcraft *et al.*, 2003).

The ~~data set of~~ wind dataset was provided by the National ~~Climate Data Center (NCDC) (https:// www.ncdc.noaa.gov/data-access/marineocean-data/blended-global/blended-sea-winds).~~Centers for Environmental Information (NCEI). The ~~data set~~dataset merges multiple satellite ~~observation,~~ observations with *in situ* instrument and related individual products~~. It~~, provides 6-~~hours~~h, daily, and monthly wind and climate data with a spatial resolution of 0.25°×0.25°~~. The data~~

Formatted: Font: Times New Roman
Formatted: Indent: First line: 2 ch
Formatted: Highlight
Formatted: Highlight
Formatted: Highlight
Formatted: Highlight
Formatted: Highlight
Formatted: Indent: First line: 0.74 cm
Formatted: Font: Italic, Highlight
Formatted: Font: Italic, Highlight
Formatted: Highlight
Formatted: Font: Times New Roman

set, and contains globally gridded ocean surface vector winds and wind stresses (Zhang *et al.*, 2006).

Sea surface temperature (SST) data ~~comes~~are from ~~Remote Sensing System (RSS; The download websites: http://www.remss.com/measurements/sea-surface-temperature/). The data set~~remote-sensing systems (RSSs). The dataset merges the near-coastal capability and high spatial resolution of ~~the~~ infrared SST data with through-cloud capabilities of ~~the~~ microwave SST data, and has applied atmospheric corrections. It provides daily data with a spatial resolution of ~~9km×9km~~9 km×9 km from July 1, 2002 to the present.

2.2 Methods

2.2.1 Eddy energetic and hydrodynamic instability formula

The formation mechanisms of mesoscale eddies in the ocean are commonly attributed to baroclinic and barotropic instabilities (Pedlosky, 1987~~; Zhang et al., 2015; Zhang et al., 2017).~~). The barotropic conversion (BT) and ~~the~~ baroclinic conversion (BC) are manifestations of the baroclinic and barotropic instabilities, respectively, and they are the major eddy energy sources around the LS (Yang *et al.*, 2013; Zhang *et al.*, 2013, 2015, 2017). In addition, the wind-stress work (WW) can also contribute to the formation of eddies (Ivchenko, 1997; Sun *et al.*, 2015). The BT, BC, and WW can be expressed as follows (Ivchenko, 1997; Oey, 2008):

$$BT = -\int\left(\overline{u'^{2}}\frac{\partial\bar{u}}{\partial x} + \overline{v'^{2}}\frac{\partial\bar{v}}{\partial y} + \overline{u'v'}\frac{\partial\bar{u}}{\partial y} + \overline{u'v'}\frac{\partial\bar{v}}{\partial x}\right)dz, \quad (1)$$

$$BC = -\int\frac{g^2}{\rho_0^2 N^2}\left(\overline{u'\rho'}\frac{\partial\bar{\rho}}{\partial x} + \overline{v'\rho'}\frac{\partial\bar{\rho}}{\partial y}\right)dz, \quad (2)$$

$$WW = \frac{1}{\rho}\left(\overline{u'\tau'_x} + \overline{v'\tau'_y}\right), \quad (3)$$

~~where~~Where t is ~~the~~ time; $u, v,$ and w are the zonal velocity, meridional velocity, and vertical velocity, respectively, and their positive directions are east, north, and up, respectively. g is the acceleration due to gravity; N is the buoyancy frequency; ρ is the density of sea water; ~~ρ_0~~ ρ_0 =

Formatted: Font: Italic

Formatted: Indent: First line: 0.74 cm

Formatted ...

Formatted: Font: (Intl) Cambria Math

Formatted ...

Formatted: Font: (Intl) Cambria Math

Formatted ...

Formatted: Font: (Intl) Cambria Math

Formatted ...

Formatted: Indent: First line: 1 ch

Formatted: Font: (Intl) Cambria Math

Formatted: Font: (Intl) Cambria Math

Formatted: Font: (Intl) Cambria Math

Formatted: Font: (Intl) Cambria Math

Formatted: Font: (Intl) Cambria Math

Formatted: Font: (Intl) Cambria Math, Highlight

~~$1030kg$~~$1030\ kg \bullet m^{-3}$ is the mean sea~~-~~water density; p is the sea pressure; and τ_x and τ_y are the zonal and meridional components of the wind stress, respectively. $x, y,$ and z are the conventional east-west, north-south, and up-down Cartesian coordinates, respectively. The depth integrals for BT and BC are from ~~400m~~400 m to the sea surface. The overbar denotes a time ~~averaged~~average over ~~an n-day period~~70 d, the primes denote deviations from the average value of 35 d before and after this day, and the other symbols and notations are standard. ~~The n-day period was chosen to be 70 days according to the~~From Figures ~~7~~6 and ~~9, which show~~8, it can be seen that the ~~period of the~~ counter-rotating eddy ~~-~~pair phenomenon occurs, develops, and disappears from t = −36 to t = 36, i.e., approximately 70 d. Therefore, the period is ~~close~~chosen to be 70 d. We have made several attempts to ~~70 days.~~set the period between 65 and 80 d, and they will not affect our basic conclusion. BT and BC were calculated from ~~the~~ HYCOM data. CMEMS surface~~-~~current velocity data and NCDC wind data were used to calculate ~~the~~ WW.

2.2.2 Vorticity budget equation

To examine the influence of the vorticity change, we applied the vorticity budget equation~~:~~ (Muller,1995; Kuo and Tseng, 2021):

$$\frac{\partial\zeta}{\partial t} = -u\frac{\partial\zeta}{\partial x} - v\frac{\partial\zeta}{\partial y} - (\zeta + f)\nabla \bullet \vec{u} - v\frac{\partial f}{\partial y} + \frac{1}{\rho^2}\left(\frac{\partial\rho}{\partial x}\frac{\partial P}{\partial y} - \frac{\partial\rho}{\partial y}\frac{\partial P}{\partial x}\right) - \upsilon\frac{\partial^2\zeta}{\partial^2 z}, \qquad (4)$$

Where $\zeta = \frac{\partial v}{\partial x} - \frac{\partial u}{\partial y}$ is the relative vorticity~~;~~, ~~t~~ t is ~~the~~ time~~; u and v,~~ f is the ~~zonal velocity, meridional velocity, respectively. $x, y,$ and z are the conventional east-west, north-south and up-down cartesian coordinates, respectively; f is the~~ Coriolis parameter~~; ρ is the sea water density;~~, P is the sea~~-~~water pressure~~;~~, and $\upsilon = 1.004 \times 10^{-6}$ is the kinematic viscosity coefficient. $x, y, z, u, v,$ and ρ in formula (4) are as defined in formulas (1)-(3). The items on the right-hand side of the equation are, from left to right, the zonal advection ~~term, the~~, meridional advection ~~term,~~

Formatted: ...
Formatted: ...
Formatted: ...
Formatted: Indent: First line: 0.74 cm
Formatted: Highlight
Formatted: ...
Formatted: ...
Formatted: ...
Field Code Changed: ...
Formatted: ...
Formatted: Font: (Intl) Cambria Math
Formatted: Font: (Intl) Cambria Math, Highlight
Formatted: Font: (Intl) Cambria Math
Field Code Changed

~~the~~, stretching ~~term, the~~, beta ~~term, the~~, baroclinic ~~term~~, and ~~the~~ diffusion ~~term from left to right.~~ terms.

2.2.3 Definition of modes and intensity index of counter-rotating eddy-pair phenomenon

When an AE (a CE) in the NWP gradually approaches the northern LS, a CE (an AE) gradually forms on the west side of the LS, and we define it as an AE (a CE) mode of the counter-rotating eddy-pair phenomenon, as shown in Figures 2a, 3a, and 6 (Figures 2b, 3b, and 8).

To reflect the intensity of counter-rotating eddy-pair phenomenon, we must construct an intensity index. As this phenomenon mainly involves the difference of SSHA between the east and west sides of the LS, the index is defined as the time series of the SSHA in the east red box of Figure 2 (expressed as $SSHA_{east}$) minus that in the west red box of Figure 2 (expressed as $SSHA_{west}$), which is shown in Figure 3a and can be expressed as $Index = SSHA_{east} - SSHA_{west}$.

3 Results

3.1 Identification of ~~and temporal variation in the~~ counter-rotating eddy pair in ~~the~~ LS

~~—~~Based on cluster analysis, which is the same as the clustering method used by Sun *et al.* (2018), ~~we determined~~ the SSHA and sea~~-~~temperature anomaly (STA) are determined based on the days when an AE and a CE ~~existed~~exist on the east side ~~and west side~~ of the LS (shown in the white box in Figure 1), respectively. Figure ~~3 shows that when an AE (a CE) occurred on the east side of the LS, a CE (an AE) formed on the west side of the LS, which is defined as a counter-rotating eddy pair in the LS in this paper. Figure 3a~~2a shows that the SSHA in the red box on the east side of the LS ~~increased~~increases from the outside to ~~the~~ inside, which means that there ~~was~~is an AE. ~~Due~~Owing to ~~the~~ geostrophic balance and mass conservation, the AE causes convergence of ~~the~~ sea water, leading to ~~downwelling~~down-welling in its center, subsequently leading to an increase in the

Formatted: Pattern: Clear (White)
Formatted: Highlight
Formatted: Highlight
Formatted: Highlight
Formatted: Indent: First line: 0.74 cm
Formatted: Font: Italic
Formatted: Highlight

temperature in the deep ocean. This is verified by the fact that the STA in the red box on the east side of the LS ~~is~~ gradually increases from outside to inside and the value is ~~the~~ highest in the center. In addition, the SSHA in the red box on the west side of the LS decreases from outside to inside and the STA is negative, indicating the presence of a weak CE. ~~Figure 3b is similar to Figure 3a, but for a CE and an AE on the east and west sides of the LS, respectively~~According to the definition of modes of the counter-rotating eddy pair given in Section 2.2.3, the SSHA pattern in Figure 2a can be identified as an AE mode of the counter-rotating eddy pair.

~~In order~~Figure 2b is similar to ~~better reflect the~~ Figure 2a, but for a CE and an AE on the east and west sides of the LS, respectively, its SSHA pattern can be identified as an AE mode of the counter-rotating eddy pair. According to the intensity ~~of this phenomenon, we~~ index defined in Section 2.2.3, the SSHA is constructed ~~an index which is defined as the time series of the SSHA in the red box on the east side of the LS minus that on the west side of the LS, in order to obtain a time series (Figure 4a). We constructed the SSHA~~ based on the days when the positive and negative intensity index values ~~were~~are more than one standard deviation ~~away~~ from the mean~~. An~~, as shown in Figures 3b and 3c. Figure 3b (3c) shows that an AE (a CE) on the east side of the LS ~~and~~ corresponds well to a CE (an AE) on the west side of the LS ~~are shown in Figure 4b (Figure 4c) for the days with~~ , and can well reflect the AE (CE) mode of a counter-rotating eddy pair in the LS. It also shows that we can well identify this phenomenon according to the intensity index, and, furthermore, that the positive ~~(~~and negative~~)~~ intensity ~~index values, which reflects the~~indexes correspond to AE and CE modes, respectively, of this phenomenon ~~of a counter-rotating eddy pair in the LS well. The pattern in~~ .

Formatted: Highlight

Formatted: Highlight

Formatted: Highlight

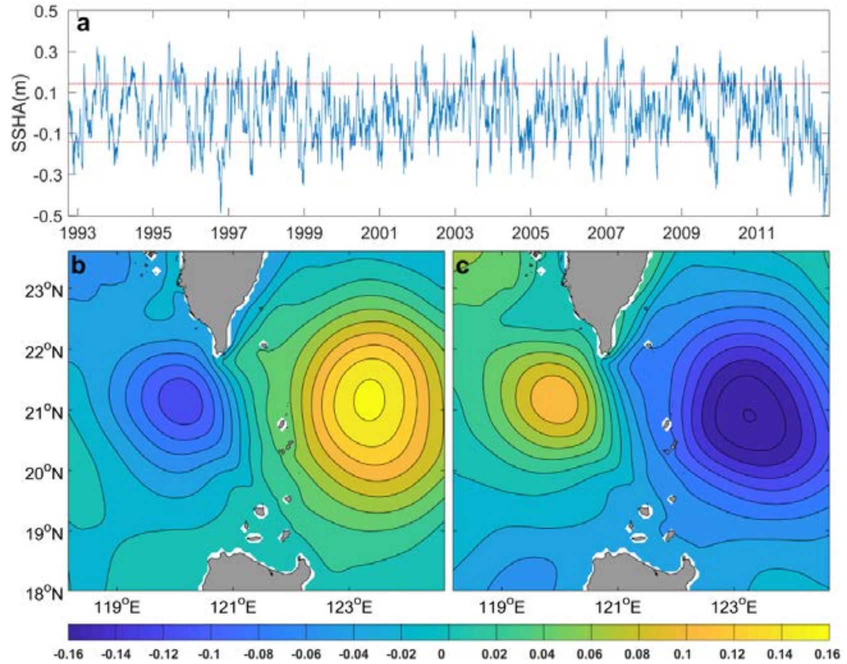

Figure ~~4b (Figure 4c) is defined as the AE (CE) mode of the counter-rotating eddy pair in this paper.~~

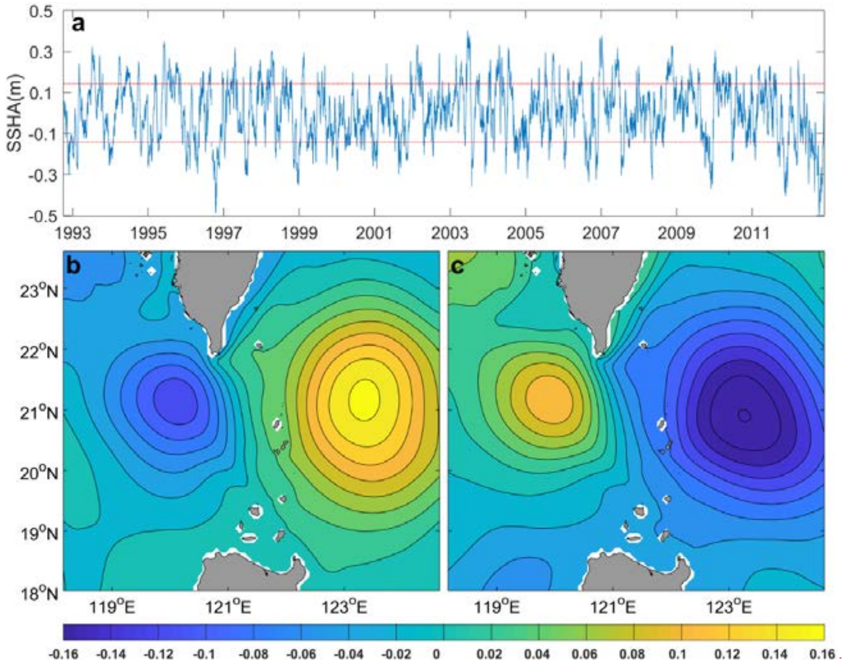

~~Figure 4. (a)~~3. Time series of ~~the~~ intensity index of ~~the~~ counter-rotating eddy pair in ~~the~~ LS~~. The red (a).~~ Red dotted line above (below) represents the sum (difference) of one time the standard deviation and the average value of the time series. Composition of ~~the~~ SSHA for ~~(b) the~~ positive (b) and negative (c) intensity ~~-~~index days ~~and (c) the negative intensity index days. The~~. SSHA interval ~~of the SSHA~~ is 0.02 m. ~~This figure is~~Figure based on HYCOM data.

3.2 Seasonal variation of counter-rotating eddy pair in LS

We counted the temporal distribution of the positive and negative intensity index values~~.~~ in a statistical sense. Figure ~~5a (Figure 5b~~4a (4b) shows that most of the AE (CE) mode of the instances of the counter-rotating eddy pair ~~occurred~~occur in the summer (winter) half of the year. The first two months with the highest incidences of the AE (CE) mode ~~occur were~~are May and June (December and January), and their occurrence rates ~~were~~are 17.01% and 15.47% (19.69% and 15.57%), respectively. We constructed the geostrophic current in May and June (Figure ~~6a~~5a) and

Formatted: Highlight
Formatted: Highlight
Formatted: Highlight
Formatted: Highlight
Formatted: Highlight
Formatted: Indent: First line: 2 ch
Formatted: Highlight

in December and January (Figure ~~6b~~5b). The patterns of the Kuroshio Current in Figures ~~6a~~5a and ~~6b~~5b exhibit as the “Leap” and “Loop” patterns of the Kuroshio in the LS, which illustrates that the Leap and Loop patterns of the Kuroshio contribute to the occurrence of the AE ~~mode~~ and ~~the~~ CE ~~mode~~modes, respectively, of the counter-rotating eddy pair~~, respectively.~~. Figure ~~6c (Figure 6d~~5c (5d) shows that the geostrophic current anomaly in the northern LS is northward (southward). It produces ~~produce~~ positive (negative) vorticity through horizontal velocity shear on the west side of the LS, and then contributes to the formation of a CE (an AE) on the west side of the LS. We ~~will~~ discuss the dynamic mechanism of the counter-rotating eddy~~-~~pair phenomenon in detail in Section 3.3.~~–~~

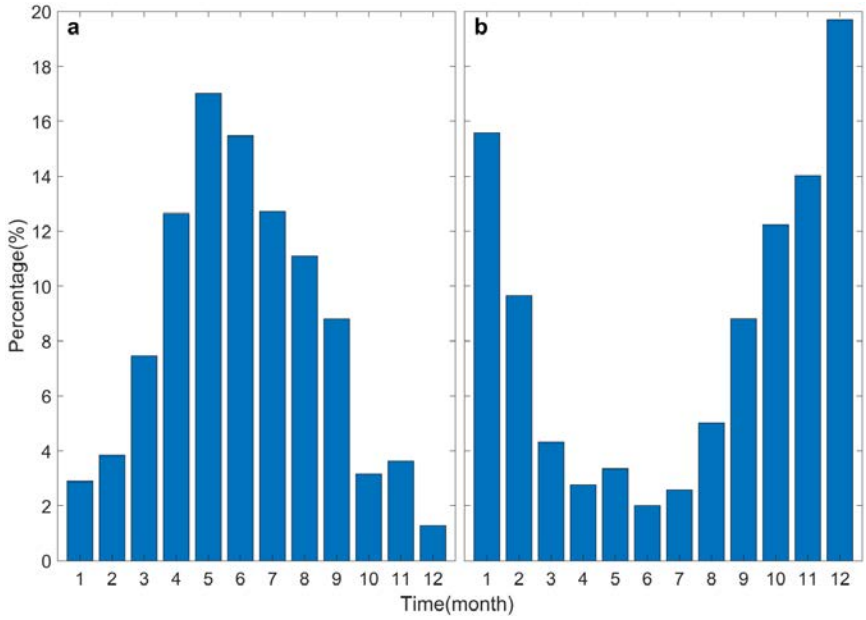

Figure ~~5~~4. Seasonal distribution of ~~the~~ occurrence rate for ~~(a) the~~ positive ~~intensity index~~ (a) and ~~(b)~~ ~~the~~ negative (b) intensity ~~index~~indexes.

Formatted: Highlight

Formatted: Highlight

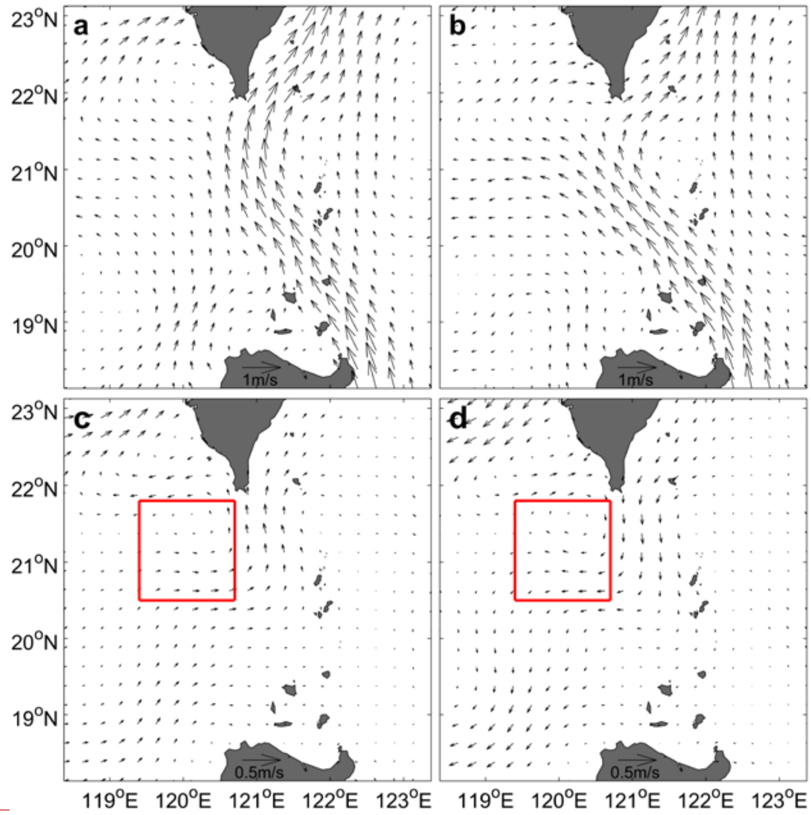

Figure 65. Climatic distributiondistributions of the geostrophic current in (a) May and June; (a) and (b)in December and January; Climatic distribution of the (b), and of geostrophic current anomaly in (c) May and June; (c) and (d)in December and January. The red (d). Red boxes in the (c) and (d) outline 20.5-–21.8°N, 119.4-–120.7°E, which representsrepresent the position of the mesoscale eddies on the west side of the LS. The figure is Figure based on CMEMS data.

3.23 Evolution of the counter-rotating eddy pair in the LS

Figure 76 shows the spatial evolution of the AE mode of the counter-rotating eddy pair in the LS. It shows that at the beginning, for example, at t = -–24, there wasis a weak AE far away from the east side of the LS, but there was no CE on the west side of the LS. From t = -–20 to t = 0,

Formatted: Centred

Formatted: Highlight

Formatted: Highlight

Formatted: Highlight

Formatted: Indent: First line: 0.74 cm

Formatted: Highlight

as the AE in the NWP ~~approached~~approaches the northern LS, a CE gradually ~~formed~~forms on the west side of the LS. At t = 0, the AE mode ~~reached the pinnacle.~~reaches its maximum. Then, from t = 4 to t = 36, as the AE in the NWP gradually ~~moved~~moves away from ~~to~~ the northern LS, the CE on the west side of the LS gradually ~~weakened~~weakens until it finally ~~died~~dies out.

The growth and weakening of a mesoscale eddy must be accompanied by a change in its relative vorticity. Figure ~~8a~~7a shows that as the AE on the east side of the LS ~~approached~~approaches and then ~~moved~~moves away from the northern LS, its relative vorticity initially ~~decreased first~~decreases and ~~increased~~then increases, while the relative vorticity of the corresponding CE on the west side of the LS initially ~~increased~~increases and then ~~decreased~~decreases. The maximum negative (positive) value of the time series of the AE (CE) on the east (west) side of the LS ~~reached~~ reaches -4.2×10^{-6} s^{-1} (3.6×10^{-6} s^{-1}). These time series ~~had a~~have good correspondence~~,~~ and their correlation coefficient ~~was~~ is −0.97 at the 95% confidence level. Therefore, the temporal variations in the relative vorticity in Figure ~~8a~~7a verify the evolution of the AE mode of the counter-rotating eddy pair in the LS.

Formatted: Highlight

Formatted: Highlight

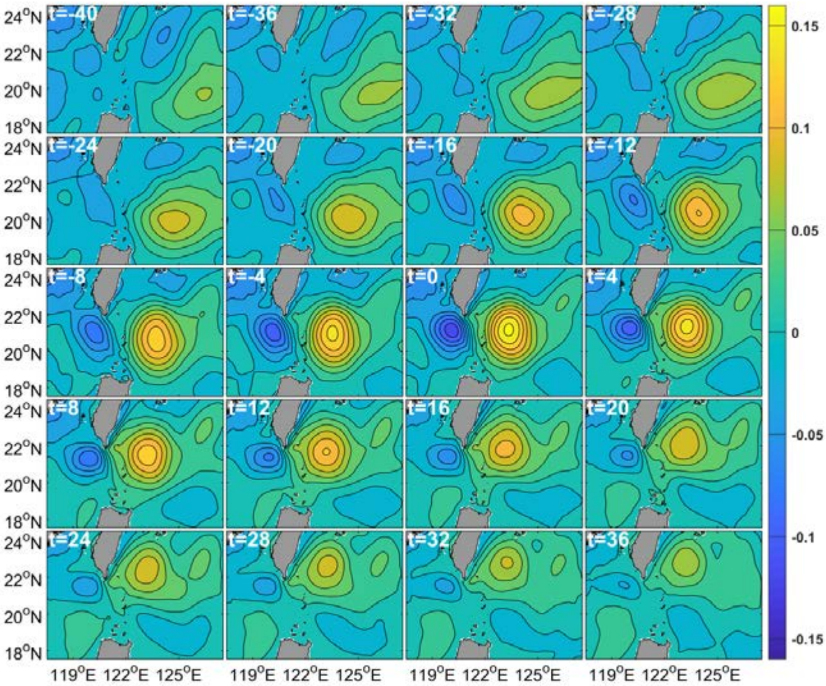

Figure ~~7~~6. Evolution of ~~the~~ AE mode of ~~the~~ counter-rotating eddy pair in ~~the~~ LS based on HYCOM data. ~~The contours~~Contours and shading both represent ~~the~~ SSHA (~~unit:~~units of m). ~~The~~SSHA interval ~~of the SSHA~~ is 0.02 m. ~~The~~ t value in the top-~~ ~~left-hand corner of each panel denotes the days before (negative value) or after (positive value) ~~the~~ AE mode of ~~the~~ counter-rotating eddy pair reached the ~~pinnacle~~maximum (t=0). t = 0 corresponds to the time of ~~the~~ Figure ~~4b.~~ 3b.

Formatted: Highlight

Formatted: Highlight

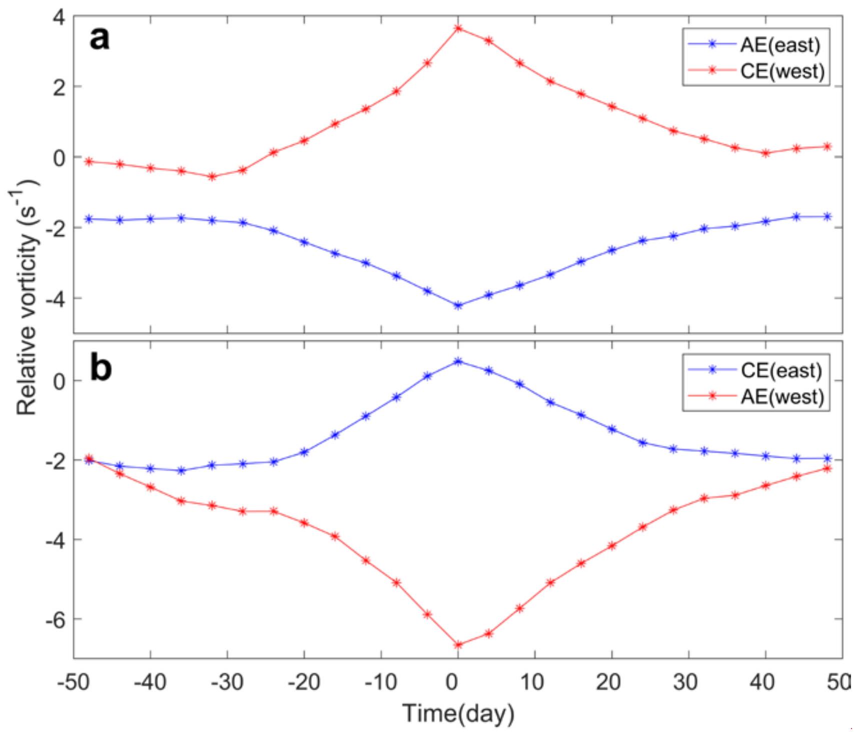
a
AE(east)
CE(west)
b
CE(east)
AE(west)
Relative vorticity (s^{-1})
Time(day)
4
2
0
-2
-4
-6
-50
-40
-30
-20
-10
0
10
20
30
40
50

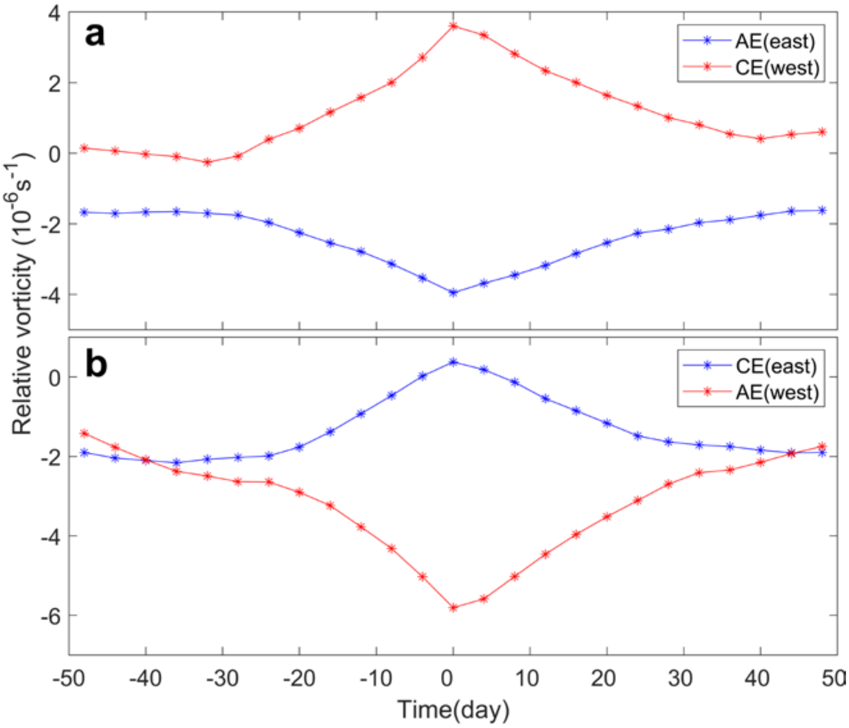

Figure ~~8. The distribution~~7. Distribution of ~~the~~ relative vorticity ~~surrounded~~in area bordered by ~~the~~ red boxes in Figure ~~3. (~~2. Panel a~~) Relative~~, relative vorticity of ~~the~~ AE mode over time. ~~The blue~~Blue (red) line represents ~~the~~ time series of ~~the~~ relative vorticity of ~~the~~ AE (CE) on ~~the~~ east (west) side of ~~the~~ LS, which corresponds to Figure ~~7; (~~6. Panel b~~) Relative~~, relative vorticity of ~~the~~ CE mode over time. ~~The blue~~Blue (red) line represents ~~the~~ time series of ~~the~~ relative vorticity of ~~the~~ CE (AE) on ~~the~~ east (west) side of ~~the~~ LS, which corresponds to Figure ~~9. This figure is~~ 8. Figure based on HYCOM data.

Formatted: Highlight

Formatted: Highlight

~~Figure 9 is the same as~~ Figure ~~7 but for~~8 plots the CE mode of the counter-rotating eddy pair in the LS. It shows that at the beginning, for example, at t = ~~-~~–32, there ~~was~~is a weak CE far ~~away~~ from the east side of the LS, but ~~there was~~ no ~~an~~ AE on the west side of the LS. From t = ~~-~~–28 to t

= 0, as the CE in NWP ~~approached~~approaches the northern LS, an AE gradually ~~formed~~forms on the west side of the LS. At t = 0, the CE mode of the evolution of the counter-rotating eddy pair ~~reached~~reaches the ~~pinnacle~~maximum. Then, from t = 4 to t = 36, as the CE in the NWP gradually ~~moved~~moves away from the northern LS, the AE in the west side of the LS gradually ~~weakened~~weakens until it finally ~~died~~dies out. Figure ~~8b is the same as Figure 8a but for~~7b plots the CE mode~~. It~~ and shows that as the CE on the east side of the LS ~~approached~~approaches and ~~moved~~moves away from the northern LS, its relative vorticity initially ~~increased~~increases and then ~~decreased;~~decreases, while the relative vorticity of the corresponding AE on the west side of the LS initially ~~decreased~~decreases and then, ~~increased~~increases. The maximum positive (negative) value of the time series of the CE (AE) on the east (west) side of the LS can reach 0.48$\times10^{-6}$ s^{-1} ~~(–~~ (−6.7$\times10^{-6}$ s^{-1}). These time series ~~had a~~have good correspondence and their correlation coefficient ~~was~~ is −0.96 at the 95% confidence level. Therefore, the temporal variations in the relative vorticity in Figure ~~8b~~7b verify the evolution of the AE mode of the counter-rotating eddy pair in the LS. The evolution of the AE ~~(~~and CE~~) mode~~ modes of the counter-rotating eddy pair in the LS is also reflected by the satellite observations (Figures ~~10~~9 and ~~11~~10).

Formatted: Highlight

Formatted: Superscript

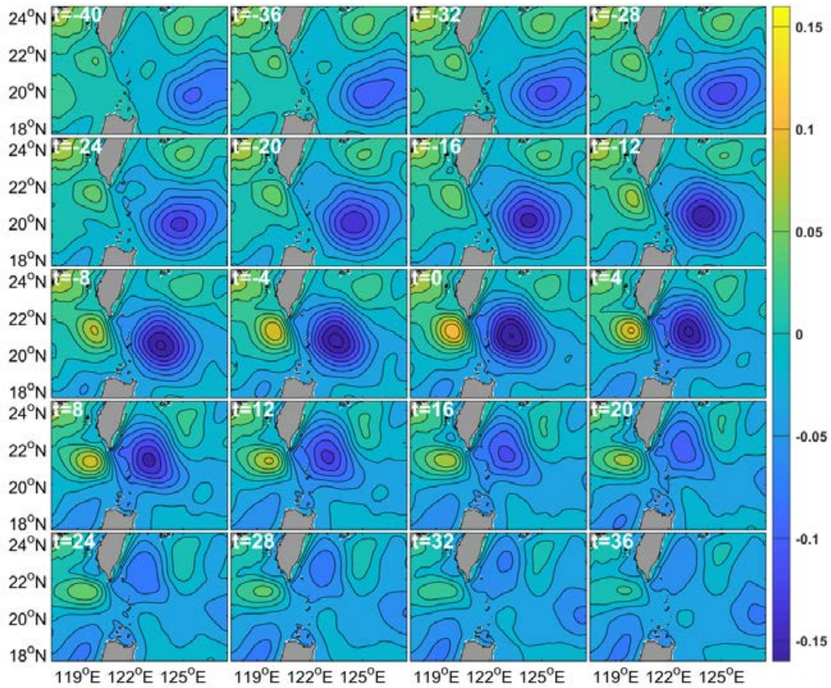

Figure 9 is the same as Figure 7 but for the CE mode of the counter-rotating eddy pair in the LS.

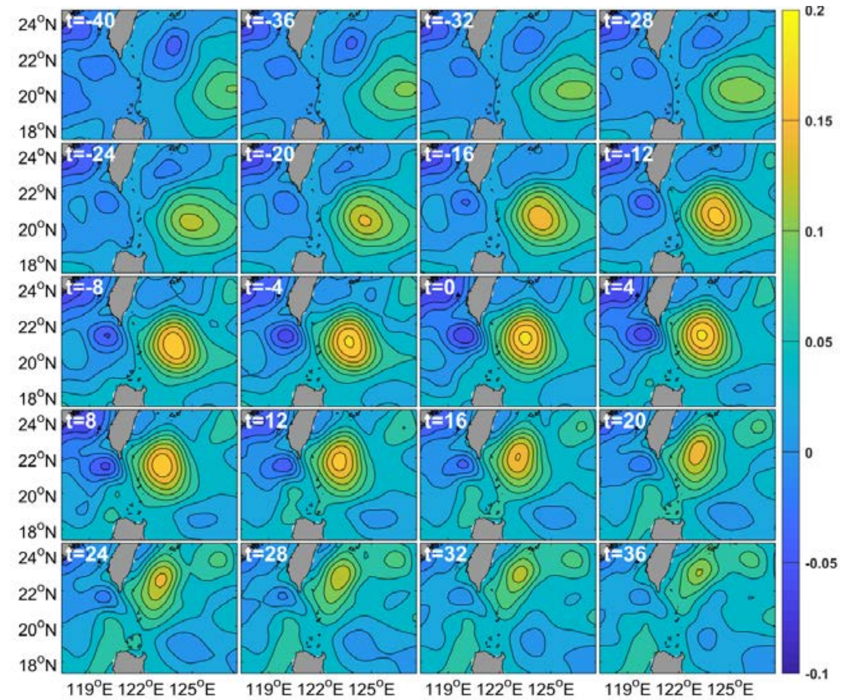

~~Figure10 is the same as Figure 7, but it is based on the CMEMS data.~~

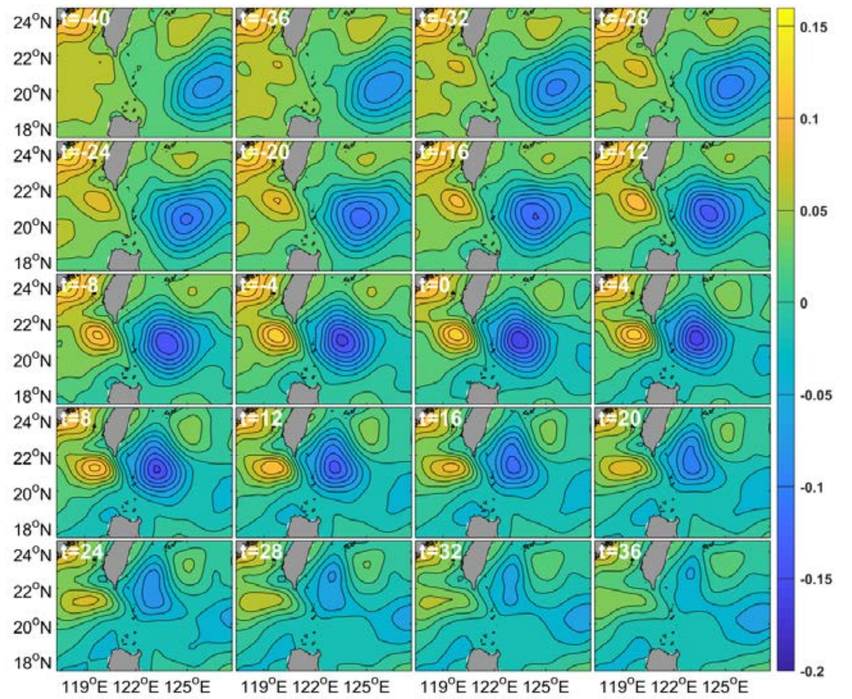

~~Figure 11 is the same as Figure 9, but it is based on the CMEMS data.~~

Figure 8 Evolution of CE mode of counter-rotating eddy pair in LS based on HYCOM data. Contours and shading both represent SSHA (units of m). SSHA interval is 0.02 m. t in the top left-hand corner of each panel denotes the days before (negative value) or after (positive value) the CE mode of the counter-rotating eddy pair reached the maximum (t=0). t = 0 corresponds to time of Figure 3b.

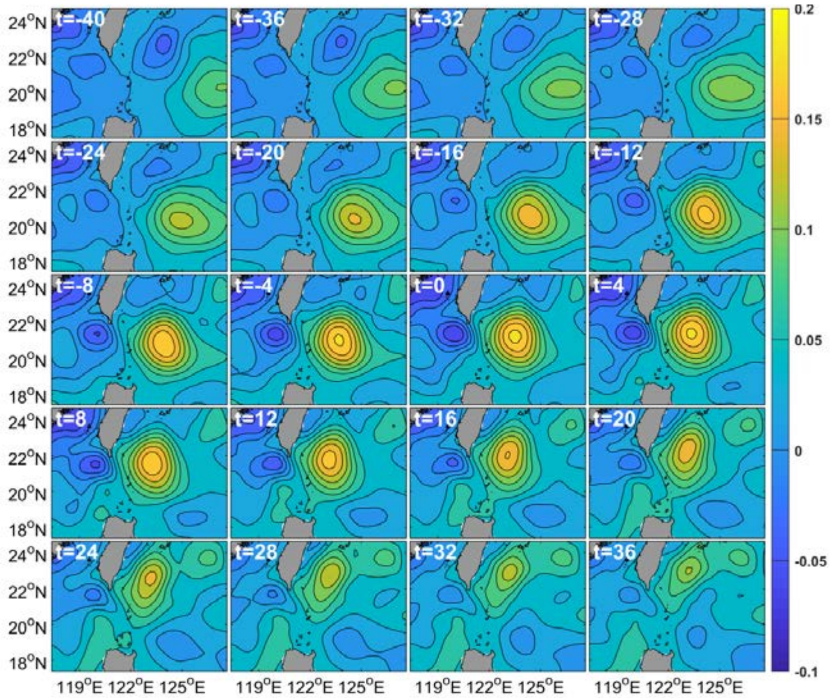

Figure 9 Evolution of AE mode of counter-rotating eddy pair in LS based on CMEMS data. Contours and shading both represent SSHA (units of m). SSHA interval is 0.02 m. t in the top left-hand corner of each panel denotes days before (negative value) or after (positive value) the AE mode of counter-rotating eddy pair reached the maximum (t=0). t = 0 corresponds to time of Figure 3b.

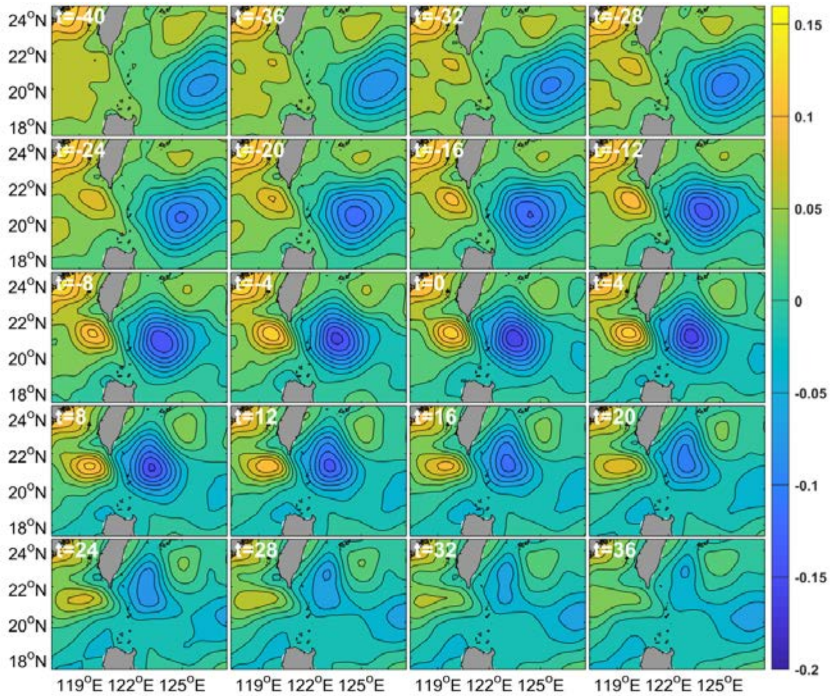

Figure 10 Evolution of CE mode of counter-rotating eddy pair in LS based on CMEMS data. Contours and shading both represent SSHA (units of m). SSHA interval is 0.02 m. t in the top left-hand corner of each panel denotes days before (negative value) or after (positive value) the CE mode of counter-rotating eddy pair reached the maximum (t=0). t = 0 corresponds to time of Figure 3b.

3.~~3~~4 Formation mechanism of ~~the~~ counter-rotating eddy pair in ~~the~~ LS

Zhang *et al.* (2017) reported that CEs mainly ~~form~~formed due to the barotropic instability caused by horizontal velocity shear of the Kuroshio Loop current southwest of ~~the~~ Taiwan Island. Huang *et al.* (2019) discovered that an AE from the NWP caused a CE to form on the west side of the LS via horizontal velocity shear. In addition, Figures ~~4b~~3b and ~~4c~~3c show that the dense contour of the SSHA means that there ~~were~~are strong current anomalies and thus strong horizontal velocity shear at the junction of the AE and CE. Therefore, we investigated the role of horizontal velocity

Formatted: Indent: First line: 0.74 cm

Formatted: Font: Italic

Formatted: Font: Italic

shear in the formation of a counter-rotating eddy in the LS.

Because meridional horizontal velocity shear is weak, we only show the zonal velocity shear. Figure 1211 shows that from t = --40 to t = 0, as the AE on the east side of the NWP gradually approachedapproaches the northern LS, the absolute value of the zonal horizontal velocity shear ($\frac{\partial v}{\partial x}$ $\frac{\partial v}{\partial x}$) gradually increasedincreases, and a CE gradually formedforms and strengthenedstrengthens on the west side of the LS. From t = 0 to t = 36, as the AE gradually movedmoves away from the northern LS, the absolute value of the zonal horizontal velocity shear gradually decreaseddecreases, and the CE on the west side of the LS gradually weakened. Figure 13 is the same asweakens. Figure 12, but for plots the CE mode of the counter-rotating eddy pair in the LS. It and shows a similar corresponding evolution process. This demonstrates that there is a good correspondence between the zonal horizontal velocity shear and the evolution process of the counter-rotating eddy pair.

Field Code Changed

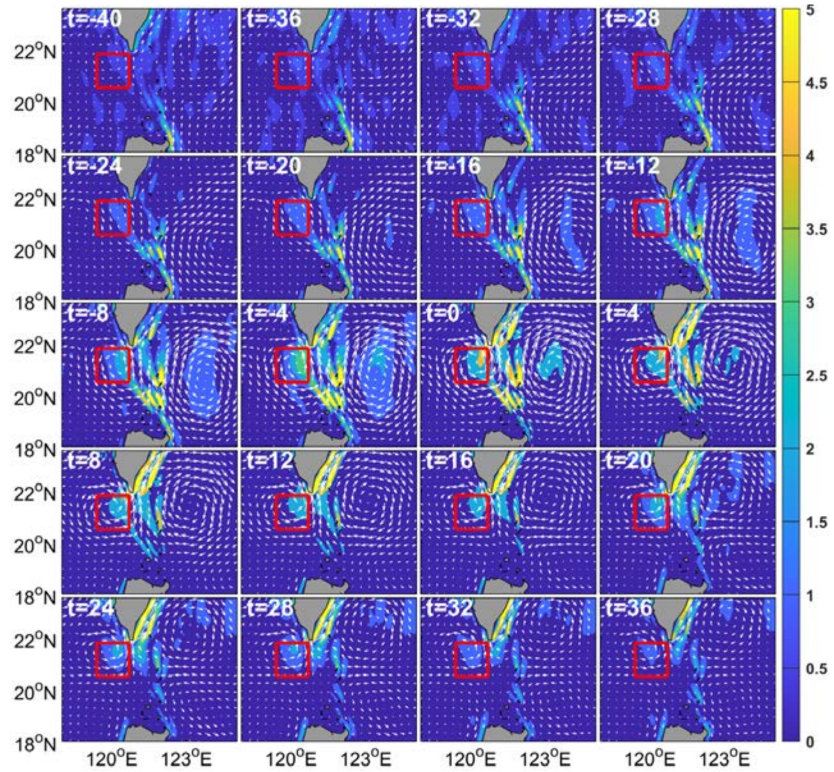

Figure ~~12~~11 Evolution process of ~~the~~ absolute value of ~~the~~ zonal horizontal velocity shear ($\frac{\partial v}{\partial x}$ $\frac{\partial v}{\partial x}$) for ~~the~~ AE mode of ~~the~~ counter-rotating eddy pair in ~~the~~ LS based on HYCOM data. ~~The shading~~Shading represents ~~the~~ zonal horizontal velocity shear (~~unit: 10~~^{6}units of 10^{-6} s^{-2}). ~~The vector~~Vector represents the current anomaly. ~~The~~ t in the top-left-hand corner of each panel denotes ~~the~~ days before (negative value) or after (positive value) the AE mode of ~~the~~ counter-rotating eddy pair reached the ~~pinnacle~~maximum (t = 0). ~~Time~~ t = 0 corresponds to ~~the~~ time of ~~the~~ Figure ~~4b. The red~~3b. Red boxes on ~~the~~ west side of ~~the~~ LS cover 20.5–21.8°N, 119.4–120.7°E and ~~represents the~~represent location of ~~the~~ CE on ~~the~~ west side of ~~the~~ LS.

Field Code Changed

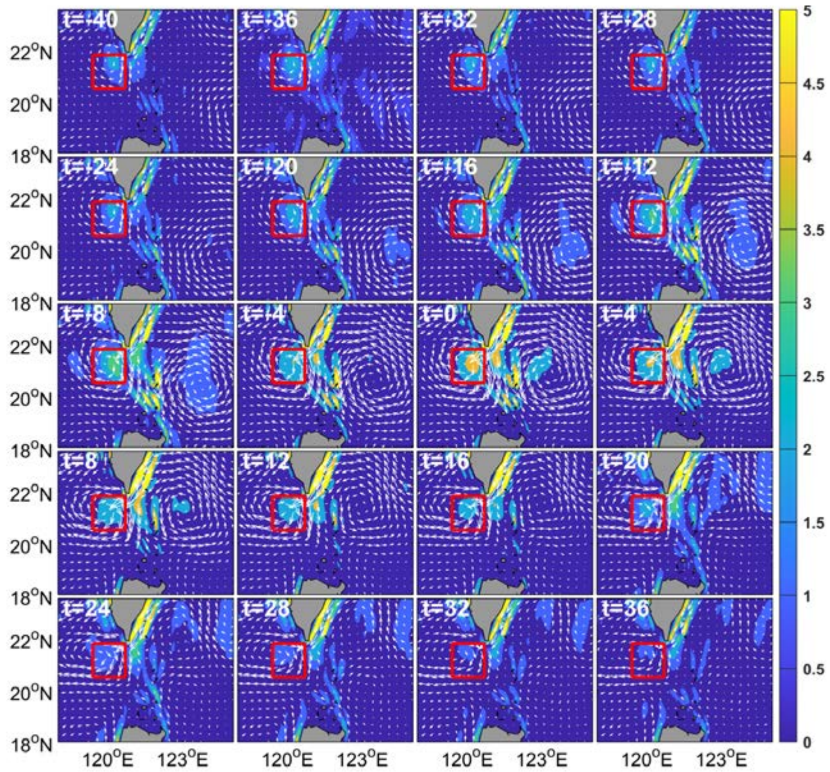

~~Figure 13 is the same as Figure 12 but for the CE mode of the counter-rotating eddy pair in the LS.~~

Figure 12 Evolution process of absolute value of zonal horizontal velocity shear ($\frac{\partial v}{\partial x}$) for CE mode of counter-rotating eddy pair in LS based on HYCOM data. Shading represents zonal horizontal velocity shear (units of $10^{-6}\,s^{-2}$). Vector represents current anomaly. t in top left-hand corner of each panel denotes days before (negative value) or after (positive value) the AE mode of counter-rotating eddy pair reached the maximum (t = 0). Time t = 0 corresponds to time of Figure 3b. Red boxes on west side of LS cover 20.5-21.8°N, 119.4-120.7°E and represent the location of CE on west side of LS.

Field Code Changed

However, Figure 11 (12 ~~(Figure 13~~) shows that zonal horizontal velocity shear only ~~occurred~~occurs on the right-hand side of the red box~~,~~; that is, on the right-hand side of the CE (AE).

How does the horizontal velocity shear pass to the entire CE (AE)? To answer this question, we used the vorticity budget equation. Figures 14 (a1 - 13a1-f1) are for plot the AE mode of the counter-rotating eddy pair and show the respective contributions of the zonal advection term, meridional advection term, stretching term, beta term, baroclinic term, and diffusion termterms of the vorticity budget equation, respectively.. Compared to the stretching term, the, beta term, baroclinic term, and diffusion termterms, the values of the zonal advection term and the meridional advection termterms in the red box are large. However, most of the values of the meridional advection term in the red box are negative. Only positive vorticity advection can lead to CE formation of a CE, which suggests that the zonal advection term is the main cause of the CE formation in the red box. To further test this conclusion, Figure 15a14a shows the correspondence between the relative vorticity anomaly and the zonal advection of the vorticity in the red box in Figure 14. It shows13, illustrating that there is a good correspondence and their correlation coefficient is as high as 0.96 at the 95% confidence level. Therefore, we conclude that the zonal advection term plays the most important role in the vorticity transport and contributes to the formation of the CE on the west side of the LS.

Figures 14 (a2 - 13a2-f2) are the same as Figures 14 (a1 - f1), but forplots the CE mode of the counter-rotating eddy pair. Figures 14 (a2 - f2) also show and shows that, compared to the stretching term, beta term, baroclinic term, and diffusion termterms, the values of the zonal advection term and the meridional advection termterms in the red box are large. However, most of the values of the meridional advection term in the red box are positive. Only negative vorticity advection can lead to AE formation of an AE, which implies that the zonal advection term is the main cause of the AE formation in the red box. To further test this conclusion, Figure 15b14b shows the correspondence between the relative vorticity anomaly and the zonal advection of vorticity. It shows, illustrating

Formatted: Highlight

Formatted: Highlight

Formatted: Highlight

Formatted: Highlight

Formatted: Highlight

Formatted: Highlight

that there is~~ a~~ good correspondence and their correlation coefficient is as high as 0.84 at the 95% confidence level. Therefore, we conclude that the zonal advection term plays the most important role in ~~the ~~vorticity transport and contributes to the formation of the AE on the west side of the LS.

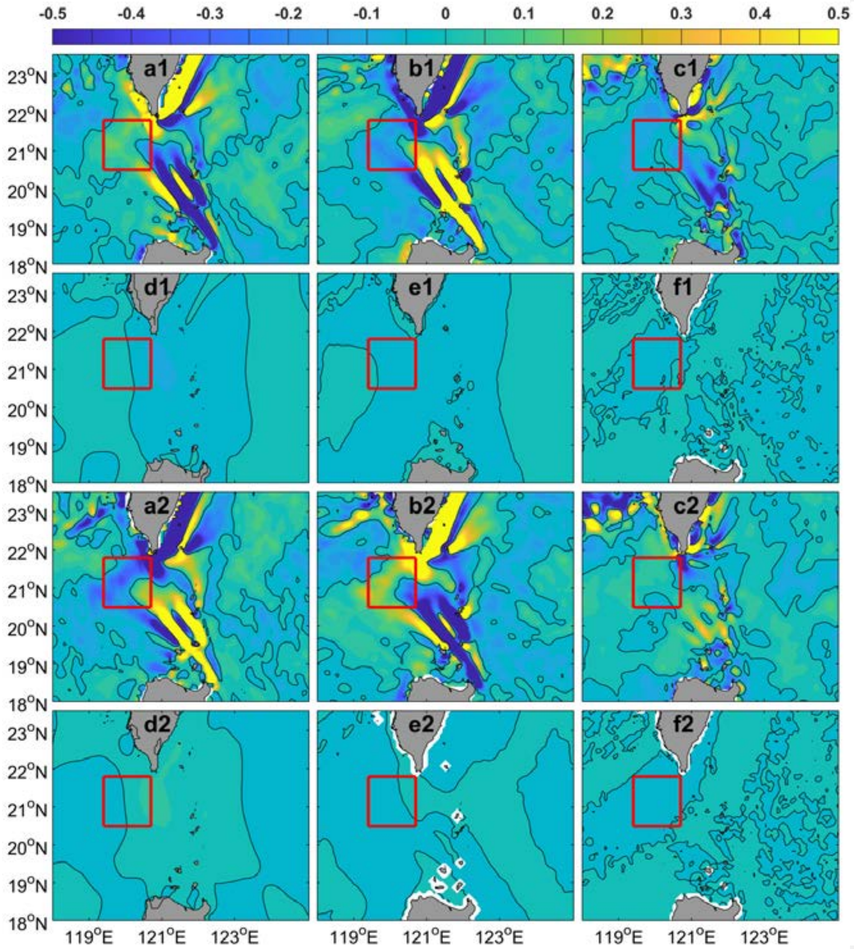

Figure ~~14~~13. Vorticity budget equation for (a1~~–~~–f1)~~ the~~ AE mode of counter-rotating eddy pair and (a2~~–~~–f2) ~~the ~~CE mode of ~~the ~~counter-rotating eddy pair. a1 and a2 represent the zonal advection term~~;~~, b1 and b2 ~~represent ~~the meridional advection term~~;~~, c1 and c2 ~~represent ~~the stretching term~~;~~, d1 and d2 ~~represent ~~the beta term~~;~~, e1 and e2 ~~represent ~~the baroclinic term~~;~~, and f1 and f2 ~~represent~~

the diffusion term. ~~The unit is 10^{10}~~Units are 10^{-10} s^{-2}. ~~The red~~Red boxes on ~~the~~ west side of ~~the~~ LS border cover 20.5–21.8°N, 119.4–120.7°E, and ~~they~~ represent ~~the~~ location of ~~the~~ CE or AE on ~~the~~ west side of ~~the~~ LS. ~~The black~~Black solid line represents the zero contour. ~~This figure is~~ Figure based on ~~the~~ HYCOM data.

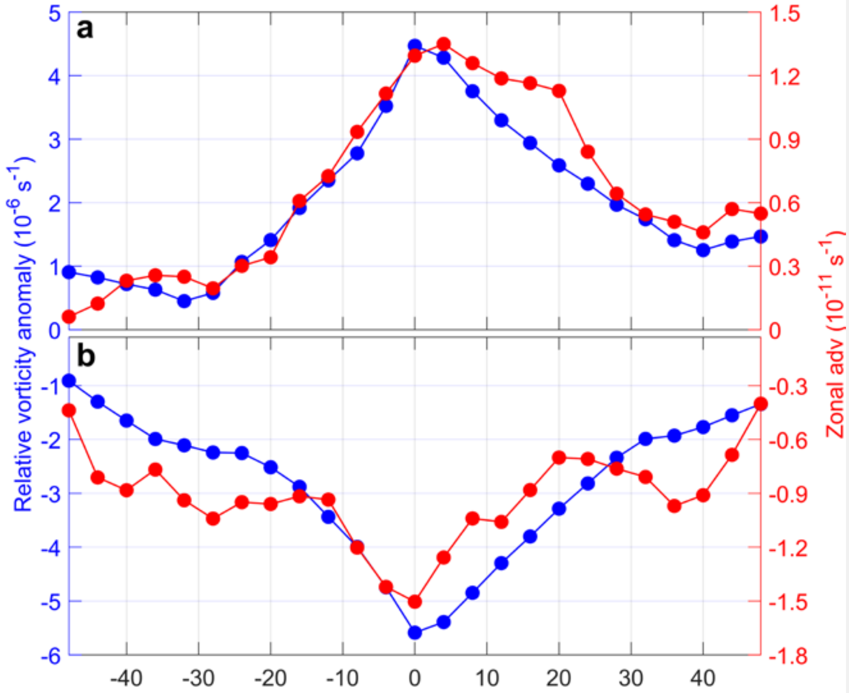

Figure ~~15. The distribution~~14. Distribution of ~~the~~ relative vorticity anomaly and ~~the~~ zonal advection of vorticity surrounded by ~~the~~ red boxes in ~~Figure14~~Figure 13 for AE (a) ~~is for the AE mode~~and CE (b) modes of ~~the~~ counter-rotating eddy pair in ~~the~~ LS~~; and (b) is for the CE mode of the counter-rotating eddy pair in the LS.~~.

~~Above, we have~~We proposed above that the horizontal velocity shear caused by the mesoscale eddy on the east side of the LS is transported westward through zonal advection, resulting in the formation of a counter-rotating mesoscale eddy on the west side of the LS. Horizontal velocity shear

Formatted: Indent: First line: 0.37 cm

will inevitably lead to barotropic instability. Now, we ~~will~~ verify our conclusion from the perspective of energy. Figures ~~16a, 16b~~15a, 15b, and ~~16c~~15c show that, compared to the BC and WW values, the BT values in the LS are large and most of the values are positive, especially in the area surrounded by the red box in Figure ~~16a~~15a, which is the junction of the AE and CE. This means that the BT plays the most important role in ~~the~~ formation of the AE on the west side of the LS.

Figures ~~16d, 16e~~15d, 15e, and ~~16f~~15f show the BT, BC, and WW, respectively, corresponding to the AE mode of the counter-rotating eddy pair in the LS~~, respectively. Its~~. The description and dynamic mechanism of the AE mode are similar to those of the CE mode of the counter-rotating eddy pair in the LS, so ~~we will discuss~~ the details ~~in this paper~~will not be discussed here.

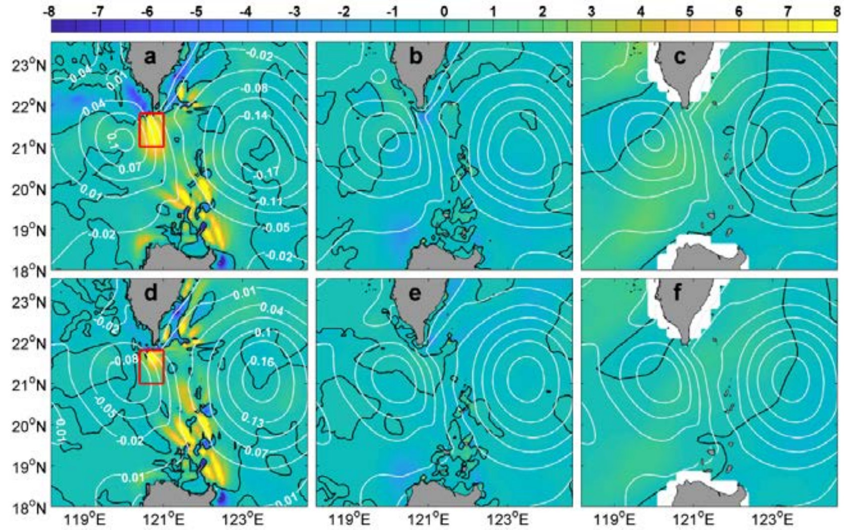

~~Figure16. (a)~~Figure 15. BT based on HYCOM data (10^{-5} ~~m^3s~~ $m^3\ s^{-3}$) represented by ~~the~~ colors~~; (b)~~ (a, d); BC based on HYCOM data (~~m^3s~~ 10^{-5} $m^3\ s^{-3}$) represented by ~~the~~ colors~~; (c)~~ (b, e); WW based on CMEMS surface velocity data and NCDC wind data (~~m^3s~~ 10^{-5} $m^3\ s^{-3}$) represented by ~~the~~ colors~~;~~ ~~The red~~ (c, f). Red box borders 21°N–21.8°N, 120.4°E–121°E. ~~The white~~White contours represent ~~the~~SSHA contours of ~~the SSHA.~~. Panels a, b, and c ~~are for the~~(d, e, and f) plot CE (AE) mode of

Formatted: Highlight

Formatted: Highlight

~~the~~ counter-rotating eddy pair in ~~the~~ LS. ~~d, e and f are for the AE mode of the counter-rotating eddy pair in the LS.~~

4 Discussion and conclusions

In this study, based on satellite observation data and HYCOM ~~reanalysis~~re-analysis data, the counter-rotating eddy pair in the LS ~~was~~is investigated. The phenomenon of counter-rotating eddy ~~pair was~~pairs is defined as the stage when an AE (a CE) in the NWP gradually ~~approached~~approaches the northern LS, and a CE (an AE) ~~formed~~forms on the west side of the LS. This phenomenon ~~exhibited~~exhibits obvious seasonal variation~~,~~; that is, the AE mode mainly ~~occurred~~occurs in the summer half of the year, while the CE mode mainly ~~occurred~~occurs in the winter half of the year. The mean durations of the AE ~~mode~~ and CE ~~mode were~~modes are both ~~about~~approximately 70 ~~days~~d. The Leap and Loop patterns of the Kuroshio ~~contributed~~Current contribute to the occurrence of the AE ~~mode~~ and CE ~~mode of the counter-rotating eddy pair~~modes, respectively~~.~~, of counter-rotating eddy pairs. Based on ~~energy analysis and~~ the vorticity budget equation and energy analysis, the dynamic mechanism of the occurrence of a counter-rotating eddy pair is as follows. The AE (CE) in the NWP causes a positive (negative) vorticity anomaly through horizontal velocity shear on the west side of the LS, and the positive (negative) vorticity anomaly is transported westward by the zonal advection of the vorticity, finally leading to the formation of a CE (an AE) on the west side of the LS. This conclusion is also verified by barotropic instability based on the energy analysis.

When we investigated the question of how the horizontal velocity shear passes to the entire CE or AE in Section 3.4, we found that the magnitudes of the meridional and zonal advection terms are roughly the same. Because the meridional advection term has the opposite effect of CE (AE)

Formatted: Indent: First line: 0.74 cm

Formatted: Highlight

Formatted: Highlight

Formatted: Highlight

Formatted

formation in the west side of the LS for the AE (CE) mode of the counter-rotating eddy pair, we confirmed that the zonal advection term plays a main role in horizontal velocity shear transportation. However, ~~the research~~since the magnitude of the meridional advection term is very large, it may play a role in the ocean dynamic process of the LS, which deserves further study.

The results presented in this ~~paper is~~study are preliminary and ~~some~~several problems require further ~~study~~research. The occurrence probability of a counter-rotating eddy pair in the LS ~~needs to~~must be determined. The counter-rotating eddy pair phenomenon involves ~~temporal-spatial~~spatiotemporal variations in two mesoscale eddies on both sides of the LS, and it is difficult to provide a quantifiable definition of this phenomenon for a single event. For example, how far apart ~~do~~must the mesoscale eddies on the east and west sides of the LS ~~need to~~ be ~~in order~~ to define them as a counter-rotating eddy pair. We preliminarily calculated that the incidence of this phenomenon ~~was about~~is approximately 5%.

Another problem to solve involves threshold of the NWP mesoscale eddies entering the SCS, and what role ~~does~~ the Kuroshio Current plays in the counter-rotating eddy~~-~~ pair phenomenon in the LS. ~~When we illustrated~~In this study, our illustration of the counter-rotating eddy pair phenomenon ~~in this study, we eliminated~~does not include the mean current field, which means that the influence of the Kuroshio ~~was eliminated.~~Current is not considered. However, the role of the Kuroshio in ~~the~~ energy transfer is still worthy of further study. Numerical simulations can be useful to address this issue. Our study provides ~~a~~ new perspective on particle and energy exchange, and further perfects the theory of particle and energy exchange between the SCS and ~~the~~ NWP.

Acknowledges

Formatted: Highlight

Formatted: Highlight

Formatted: Highlight

Formatted: Highlight

Formatted: Highlight

Formatted: Highlight

Formatted: Highlight

Formatted: Highlight

Formatted: Indent: First line: 0 ch

The authors would like to acknowledge several data sets used in this paper. Satellite remote sensing geostrophic current data and sea level anomaly were obtained from the CMEMS (https://resources.marine.copernicus.eu/?option=com_csw&view=details&product_id=SEALEVEL_GLO_PHY_L4_REP_OBSERVATIONS_008_047),, the HYCOM reanalysis data were downloaded from HYCOM organization (https://www.hycom.org/dataserver/gofs-3pt0/reanalysis),, the data set of wind was provided by National Climate Data Center (https://www.ncdc.noaa.gov/data-access/marineocean-data/blended-global/blended-sea-winds).. Sea surface temperature data comes from Remote Sensing System (http://www.remss.com/measurements/ sea-surface-temperature/).. This study was supported by National Natural Science Foundation of China (grant number 41806019), National Key R&D Program of China (2019YFD0901305), Key R&D projection of Zhejiang Province (2020C03012), National Natural Science Foundation of China (No.41776012), State Key Laboratory of Tropical Oceanography (South China Sea Institute of Oceanology Chinese Academy of Sciences) open topics (grant number LTO2011), Key R&D project of Guangdong Province (2020B1111030002), Major science and technology project of Sanya YZBSTC (SKJC-KJ-2019KY03). We thank LetPub (www.letpub.com) for its linguistic assistance during the preparation of this manuscript.

Reference

Chang M H, Tang T Y, Ho C RHuang Z, Zhuang W, Hu J, et al. Kuroshio-induced wakeObservations of the Luzon Cold Eddy in the lee of Green Island off Taiwan[J]. Journal of Geophysical Research: Oceans, 2013, 118(3):1508-1519.

Formatted: Pattern: Clear

Formatted: Pattern: Clear

~~Jia Y, Chassignet E P. Seasonal variation of eddy shedding from the Kuroshio intrusion in the Luzon Strait~~northeastern South China Sea in May 2017[J]. Journal of Oceanography, ~~2011, 67~~2019, 75(5):~~601-611~~ 415-422.

Jing C, Li L. An initial note on quasi-stationary, cold-core Lanyu eddies southeast off Taiwan Island[J]. Chinese Science Bulletin. 48(19): 2101-2107.

Kuo Y, Tseng Y. Influence of anomalous low-level circulation on the Kuroshio in the Luzon Strait during ENSO[J]. Ocean Modelling, 2021, 159, 101559.

Ivchenko V O, Treguier A M, and Best S E. A kinetic energy budget and internal instabilities in the fine resolution antarctic model, Journal of Physical Oceanography, 1997, 27:5-22.

~~Lien R~~Liu Y, Dong C, ~~Ma B, Cheng~~Guan Y ~~H~~, et al. ~~Modulation of Kuroshio transport by mesoscale eddies at~~Eddy Analysis in the ~~Luzon Strait entrance~~Subtropical Zonal Band of the North Pacific Ocean[J]. ~~Journal of Geophysical~~Deep Sea Research~~: Oceans, 2014, 119(4):2129-2142~~ Part I, 2012, 68:54-67.

Lu J, Liu Q. Gap-leaping Kuroshio and blocking westward-propagating Rossby wave and eddy in the Luzon Strait[J]. Journal of Geophysical Research Oceans, 2013, 118(3):1170-1181.

Muller P. Ertel's potential vorticity theorem in physical oceanography[J]. Reviews of Geophysics, 1995, 33(1):67-97.

Oey L Y. Loop Current and Deep Eddies[J]. Journal of Physical Oceanography, 2008, 38(7): 1426 - 1449.

Pedlosky J. Geophysical Fluid Dynamics, 1987, 2nd ed., 710 pp., Springer, N. Y.

Pujol M ~~I~~, Francoise M. Product user manual for sea level SLA products~~, 2019.06 (http://marine.copernicus.eu/)~~. Copernicus Monitoring Environment Marine Service (CMEMS), 2022, https://doi.org/10.48670/moi-00148.

Remote Sensing Systems (RSS): https://www.remss.com/measurements/ sea-surface-temperature/.

Formatted: Indent: Left: 0 cm, Hanging: 2 ch, First line: -2 ch, Don't adjust right indent when grid is defined, Line spacing: 1.5 lines, Don't adjust space between Latin and Asian text, Don't adjust space between Asian text and numbers

Formatted: Pattern: Clear

Formatted: Pattern: Clear

Formatted: Pattern: Clear

Formatted: Highlight

Formatted: Highlight

Formatted: Highlight

Sun R, Ling Z, Chen C, ~~Yan Y~~et al. Interannual variability of thermal front west of Luzon Island in boreal winter[J]. Acta Oceanologica Sinica, 2015, (34):108.

Sun R, Wang G, Chen C. The Kuroshio bifurcation associated with islands at the Luzon Strait[J]. Geophysical Research Letters, 2016a, 43(11):5768-5774.

Sun R, Gu Y, Li P, et al. Statistical characteristics and formation mechanism of the Lanyu cold eddy[J]. Journal of Oceanography, 2016b, 72(4):641-649.

Sun R, Zhai F, Gu Y. The Four Patterns of the East Branch of the Kuroshio Bifurcation in the Luzon Strait[J]. Water, 2018, 10(12).

~~Sheu W J, Wu C~~Sun R, ~~Oey L Y. Blocking and Westward Passage~~Zhai F, Zhang G, et al. Cold Water in the Lee of ~~Eddies~~the Batanes Islands in the Luzon Strait[J]. ~~Deep Sea Research Part II: Topical Studies in Oceanography, 2010, 57(19-20):0-1791.~~

~~Wang Q, Zeng L, Chen J, et al. The linkage of Kuroshio intrusion and mesoscale eddy variability in the northern South~~ Journal of Ocean University of China ~~Sea: subsurface speed maximum. Geophysical Research Letters~~, 2020, ~~47(11).~~19(6):10.

~~Yan X, Zhu X H, Pang C, et al. Effects of mesoscale eddies on the volume transport and branch pattern of the Kuroshio east of Taiwan[J]. Journal of Geophysical Research: Oceans, 2016, 121(10): 7683-7700.~~

Wallcraft A, Carroll S N, Kelly K A, et al. Hybrid Coordinate Ocean Model (HYCOM) Version 2.1 User's Guide. HYCOM consortium, 2003. Https://www.hycom.org/dataserver/gofs-3pt0/reanalysis.

Yang H, Wu L, Liu H, et al. Eddy energy sources and sinks in the South China Sea[J]. Journal of Geophysical Research Oceans, 2013, 118(9):4716-4726.

Formatted: Font colour: Custom Colour (RGB(34,34,34)), Pattern: Clear (Custom Colour (RGB(251,251,251)))

Formatted: Font colour: Custom Colour (RGB(34,34,34)), Pattern: Clear (Custom Colour (RGB(251,251,251)))

Formatted: Font colour: Custom Colour (RGB(34,34,34)), Pattern: Clear (Custom Colour (RGB(251,251,251)))

Formatted: Normal, Left, Indent: Left: 0 cm, Hanging: 2 ch, First line: -2 ch, Pattern: Clear

Formatted: Font colour: Custom Colour (RGB(34,34,34)), Pattern: Clear (Custom Colour (RGB(251,251,251)))

Formatted: Font colour: Custom Colour (RGB(34,34,34)), Pattern: Clear (Custom Colour (RGB(251,251,251)))

Zhang Z, Wang W, Qiu B. Oceanic mass transport by mesoscale eddies[J]. Science, 2014, 345(6194):322-324.

Zhang Z, Zhao W, Tian J, et al. A mesoscale eddy pair southwest of Taiwan and its influence on deep circulation[J]. Journal of Geophysical Research Oceans, 2013, 118(12):6479-6494.

Zhang Z, Zhao W, Tian J, et al. Spatial structure and temporal variability of the zonal flow in the Luzon Strait[J]. Journal of Geophysical Research Oceans, 2015, 120(2).

Zhang Z, Zhao W, Qiu B, et al. Anticyclonic Eddy Sheddings from Kuroshio Loop and the Accompanying Cyclonic Eddy in the Northeastern South China Sea[J]. Journal of Physical Oceanography, 2017, 47(6):1243-1259.

Zhang H M, Reynolds R W, Bates J J, et al. Blended and gridded high resolution global sea surface wind speed and climatology from multiple satellites: 1987-present. American Meteorological Society 2006 Annual Meeting, Vol. 2.2. Https://www.ncei.noaa.gov/products /blended-sea-winds

Zheng Q, Tai C K, Hu J, et al. Satellite altimeter observations of nonlinear Rossby eddy-Kuroshio interaction at the Luzon Strait[J]. Journal of oceanography, 2011, 67(4): 365-376.

Formatted: Highlight